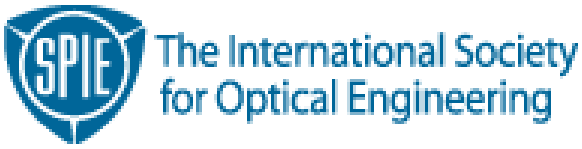

This paper was published in the proceedings of
Optical Microlithography XVII, SPIE Vol. 5377, pp. 1462-1474
and is made available as an electronic reprint with permission of SPIE.

Lumped Parameter Model for Chemically Amplified Resists

Jeffrey Byers, Mark Smith, and Chris Mack

KLA-Tencor, FINLE Division
8834 North Capital of Texas Highway, Suite 301, Austin, Texas 78759, USA

ABSTRACT

Recently the Lumped Parameter Model (LPM) has been extended to three dimensions enabling fast calculations of full resist profiles. This resist model incorporates most of the lithographically significant physical phenomenon of resist systems. This model works well to match isolated and semi-isolated line resist systems. However, it is not very successful at matching contact hole or isolated trench resist systems. The reason for this mismatch can be traced to the influence of base quencher present in chemically amplified (CA) resists yet absent from the original LPM. The quencher effectively splits the aerial image into two complementary images. These two images (acid and base) simultaneously diffuse and react with each other. A single aerial image diffusion model cannot approximate the resulting coupled quenching-diffusion system.

An improved LPM that incorporates quencher and its diffusion is presented. Successful implementation of this model requires solving the coupled quenching-diffusion system in a fast and accurate manner. Several solution methods are discussed. The agreement between the Lumped Parameter Model and a full CA resist model is greatly improved. This improvement will enable fast and more accurate calculations of resist affects on three-dimensional imaging bias.

Keywords: Lumped Parameter Model, Chemically Amplified Resist, Quencher Diffusion

1. INTRODUCTION

As critical dimensions continue to shrink the process limited yield for lithography becomes a bigger fraction of the overall process yield. This reduction in yield for currently acceptable processes improves the cost advantage of more exotic but higher yielding lithographic processes. For example off-axis illumination and attenuated phase shift masks are now mainstream but were considered rare just a few years ago. The development and implementation of these newer processes can benefit from fast but predictive lithography simulation. The chosen resist model greatly determines both the speed, accuracy, and predictability of any lithography simulation. Currently the available resist models can be classified into four groups [1]: aerial image only, empirical lumped parameter, full physical continuum, and meso/molecular scale models. Although the accuracy varies even within each class of model it is generally assumed the full physical continuum models are more accurate but slower than the aerial image and empirical lumped parameter models.

The simplest resist model considers only the aerial image. In Aerial Image Resist models the feature edge is located at any point where the intensity falls below a threshold value. Initially a constant threshold value inversely proportional to the exposure dose was used. Cobb and Zakhor [2] introduced the concept of variable threshold models in which the threshold intensity is a function of the localized image gradient. To improve accuracy the number of terms in the threshold function can be increased [3]. Unfortunately the resulting "parameters" for such models have little physical meaning. Intuition cannot be used to transfer parameters from one resist process to a slightly modified process. Recalibration is necessary for seemingly minor changes in the process. Several groups have attempted to merge specific physics into Aerial Image Resist models. Most notably are the Diffused Aerial Image Models (DAIM) [4,5] which consider the aerial image as a diffusible quantity. The diffusion length then becomes a model parameter. The aerial image is diffused either with direct Gaussian convolution or in Fourier space during the image calculation. The resist edges are then placed using the diffused aerial image and a threshold value. In DAIM the threshold value is a function of the processing conditions (Exposure dose, PEB temperature, etc) but not explicitly upon the localized aerial image function.

Further improvement in Aerial Image Resist models came when Fukuda [6] included base clipping and diffusion. In the Fukuda model the initial aerial image is quenched by a constant base image. The resulting two opposing images are allowed to diffuse and react against each other. The resist edges are then determined using a threshold function on the final unquenched aerial image. This process of two images (acid and base) diffusing against each other is an important physical concept required to match the performance of modern chemically amplified resists. Other researchers have since improved upon Fukuda's model [7,8]. These improvements average the acid image [9] during the diffusion process. The resist edge is determined based upon this average acid image instead of the final acid image. The time averaging more accurately represents the reaction-diffusion process for chemically amplified resists.

Another class of empirical resist models are the Lumped Parameter Models (LPM). The Lumped Parameter Models predate the variable threshold resist models and in the limit of very thin resist LPM reduces to an Aerial Image Resist model. Like DAIM models LPM includes empirical parameters that represent physical diffusion. Lumped Parameter Models however also include develop and image in resist effects.

The original lumped parameter model was introduced by Hershel and Mack [10] in 1987. They made two assumptions that allowed analytical calculations of the resulting resist feature width from any 1D aerial image. First, the develop rate for the resist was derived from a constant develop contrast assumption.

$$\frac{d\ln(\text{Rate})}{d\ln(\text{Dose})} = \text{contrast} = \gamma \tag{1}$$

This results in the log of the develop rate for any point in space being proportional to the log of the aerial image intensity at that location.

$$\ln(R(x,y,z)) = \gamma \cdot \ln(I(x,y,z) \cdot \text{Dose}) + \text{Constant} \tag{2}$$

or

$$R(x,y,z) = R_0 \cdot \text{Dose}^{\gamma} \cdot I(x,y,z)^{\gamma} \tag{3}$$

where the single parameter γ defines the develop rate function and R_0 is derived from the specified E_0, resist thickness and develop time. The second assumption of the original LPM was to assume a segmented develop path. Initially the resist development is propagated vertically from the nearest maximum of image intensity to the bottom of the resist. Then the development proceeds horizontally. Using these two assumptions, the original LPM model yielded a Dose-to-Size for any resist CD and 1D aerial image given by

$$\frac{\text{Dose(CD)}}{E_0} = \left(1 + \frac{1}{\text{thickness}} \int_0^{CD/2} \left(\frac{I(x)}{I(0)}\right)^{\gamma} dx\right)^{1/\gamma} \tag{4}$$

In subsequent work Mack [11] added an absorbance parameter and further assumed that the Image-in-Resist was separable into the product of the horizontal aerial image and vertical absorbance terms.

$$I(x,y,z) = I(x,y) \cdot I(z) = I(x,y) \cdot e^{-\alpha z} \tag{5}$$

This assumption coupled with the basic develop rate Equation (3) yielded better predictions of resist sidewall angles and showed how resist absorbance affects imaging performance. This improved model was termed the Enhanced Lumped Parameter Model.

Brunner and Ferguson [12] introduced two new improvements to the idea of a lumped parameter model in 1996. First, they allowed for the diffusion of the aerial image by including a Fickian diffusion length L.

$$I(x) = \frac{1}{2\pi \cdot L^2} \int_{-\infty}^{\infty} I(x - x') \cdot e^{\frac{-(x-x')^2}{2L^2}} dx' \tag{6}$$

A third segment was also added to the develop path. This third develop segment proceeded parallel to the steepest gradient of the aerial image and intersected both the vertical and horizontal components. By introducing these two improvements Brunner and Ferguson were able to improve the ability of the simplified resist model to fit focus exposure matrices across several feature width and pitch values. This work was the first time the concept of aerial image diffusion was published. Most DAIM type models that followed can be derived as simpler forms of the Brunner-Ferguson model with a simple change of parameters and the assumption of very thin resist.

The LPM has been extended to work for 3D structures [13]. A similar model was also published by another group [14]. These 3D-LPM models include defocus of the Image-in-Resist, Fickian diffusion, and solve for the generalized develop path to determine the final resist profile.

In the 3D-LPM the Image in Resist is generalized into Z and XY terms as follows

$$I(x, y, z) = \left(I_0(x, y) + I_1(x, y) \cdot z + I_2(x, y) \cdot z^2\right) \cdot e^{-\alpha z} \tag{7}$$

where $I_0(x,y)$ is the Image-In-Resist at the top of the resist, $I_1(x,y)$ is the linear change of image intensity as a function of depth, $I_2(x,y)$ is the quadratic change of image intensity as a function of depth and α is the absorbance. The image terms $I_0(x,y)$, $I_1(x,y)$, and $I_2(x,y)$ can easily be determined using three calculated images within the resist and the known absorbance. The images at the top, middle and bottom of the resist are the most convenient and effective for this model. In the absence of standing waves this simple model will effectively represent all image conditions found in lithographic systems including those with aberrations. However, because three images are now required, the Image-in-Resist calculation is slower than the simple approximation of the original LPM model, which requires just one image term. For very thin resists the image defocus and absorbance terms can be ignored and 3D-LPM reverts to an aerial image model.

This 3D Image-In-Resist is then diffused assuming simple Fickian diffusion and the develop rate everywhere is a function of the diffused Image-In-Resist.

$$R(x, y, z) = R_0 \cdot \frac{E^{\gamma}}{E_0^{\gamma}} \cdot I(x, y, z)^{\gamma} + R_{min} \tag{8a}$$

where R_{min} and γ are the develop model parameters, E_0 is the Dose to clear and E is the applied exposure energy. The R_0 parameter is redundant and easily obtained from the other model parameters. The final resist profile is computed by solving the 3D develop problem using the calculated develop rate versus position function. The 3D develop profile can be written as a line integral is which the time-to-clear every point in the resist is given as

$$\text{Time - to - Clear}(x, y, z) = T(x, y, z) = \int_0^{s_{xyz}} \frac{\sqrt{x'(s)^2 + y'(s)^2 + z'(s)^2}}{R(x(s), y(s), z(s))} ds \tag{8b}$$

where the integral is over the path variable s. The functions x(s), y(s), and z(s) describe the path. R(x,y,z) is the modeled resist develop rate as a function of position. The Principal of Least Action defines the correct path functions x(s), y(s), and z(s) as those that yield the fastest develop time for all locations in the resist. After the complete time-to-clear function is solved, the final resist profile is obtained from the locations in space with the time-to-clear equal to the develop time.

Although the 3D-LPM model works well to match a full resist model for certain resists [1] it has poor predictability for other resists. Generally it has been noticed by these authors that the LPM model works well for resists optimized for logic applications but does not have acceptable predictability for resists optimized for contact hole or isolated trench applications. Other work has shown that for chemically amplified resists, base loading and diffusion lengths are important for optimal resist design [15]. So a natural extension of the 3D LPM model is to incorporate the Fukuda base diffusion model and the subsequent enhancements by Lammers et al.

2. THEORY

A simplified kinetic model for Chemically amplified resist has been previously described and is repeated here for clarity. The reaction steps considered are shown in Figure 1.

Exposure:

$$\mathrm{PAG} + \mathrm{Light} \xrightarrow{C} \mathrm{Acid}$$

PEB:

$$\mathrm{M} + \mathrm{Acid} \xrightarrow{k_a} \mathrm{S} + \mathrm{Acid}$$

$$\mathrm{Acid} + \mathrm{Q} \xrightarrow{k_Q} \{\mathrm{Acid} - \mathrm{Q}\}$$

Figure 1: Simplified reaction steps for chemically amplified resist.

The exposure kinetics are represented by a first order reaction between the exposure light and the photoacid generator, PAG, compound. The active product of this reaction is a strong photoacid whose concentration is determined using Equation 9. This equation was first used by Dill et al. [16] to describe conventional resist photo kinetics but has subsequently been used in most chemical amplified resist models. Upon expansion into a Taylor series, this simplifies into a linear dependence for acid concentration on the product of the exposure dose and image intensity for the case of low fractional acid generation. The linear dependence is reasonably accurate for the exposure conditions found in modern chemically amplified resist applications.

$$\frac{[\mathrm{Acid}]}{[\mathrm{PAG}]_0} = \left(1.0 - e^{-C \cdot \mathrm{Dose} \cdot I}\right) = C \cdot \mathrm{Dose} \cdot I + \ldots \tag{9}$$

After exposure the resist is baked. In this post exposure bake process the acid catalytically reacts with the resist to convert insoluble resist material M into soluble resist material S. At the same time added base may quench the nearby acid catalyst rendering the acid molecule ineffective for further catalytic activity. Both the acid and base molecules diffuse during this bake process. The combined reaction and diffusion of acid and base species is represented by the coupled differential equation given in Equations 10a-c. Solving this set of reaction diffusion equations is critical to accurate modeling of chemically amplified resists.

$$\frac{d[Q]}{dt} = -k_Q \cdot [\mathrm{Acid}] \cdot [Q] + D_Q \nabla^2 [Q] \tag{10a}$$

$$\frac{d[\mathrm{Acid}]}{dt} = -k_Q \cdot [\mathrm{Acid}] \cdot [Q] + D_A \nabla^2 [\mathrm{Acid}] \tag{10b}$$

$$\frac{d[M]}{dt} = -k_a \cdot [\mathrm{Acid}] \cdot [M] \tag{10c}$$

After the post exposure bake process the resist is developed. The develop rate is a function of the fraction resist material converted into soluble species S. This soluble fraction can be obtained by integrating Equation 10c and forcing stoichiometry. The soluble fraction at any given position depends upon the integrated concentration of unquenched acid molecules.

$$S(t) = 1.0 - \frac{M(t)}{M_0} = 1.0 - \exp^{-k_a \int [Acid] dt} = k_a \int [Acid] dt + ... \tag{11}$$

In the absence of diffusion and assuming instantaneous acid-base quenching ($k_Q >> 1$) the resist soluble fraction can easily be solved to obtain Equation 12. This diffusionless resist solubile fraction is proportional to the image in resist minus the scaled base concentration ($\frac{Q}{C \cdot Dose}$). This simplification is the basis of the model presented by Fukuda. Equation 11 however requires a time integration of the acid image during diffusion to obtain the soluble resist fraction. This integration of the acid image was given in the original Lammers model [9].

$$\begin{aligned} S(I, C, Dose, k_a, Q, t) &= 1.0 - \exp^{-k_a t \cdot (1 - Q - e^{C \cdot Dose \cdot I})} \\ &\approx k_a \cdot t \cdot C \cdot Dose \cdot (I - \frac{Q}{C \cdot Dose}) \end{aligned} \tag{12}$$

A combination of the Lammers model with the LPM is presented below. This reformulation attempts to include optical, diffusion, amplification, and develop effects. The model is parameterized into a minimal set of orthogonal variables.
First, the Image-In-Resist is calculated using the LPM assumptions described in Equation 7. This requires a resist refractive index and absorbance parameter. Next the Image-In-Resist (**I**) is split into Acid ($\mathbf{I_A}$) and Base ($\mathbf{I_Q}$) components. This is illustrated in Figure 2. I_A and I_Q are obtained by completed quenching of the original Image-In-Resist profile with a constant base loading I_Q^0.

$$I_A(x, y, z) = \max\left\{I(x, y, z) - I_Q^0, 0.0\right\} \tag{13a}$$

$$I_Q(x, y, z) = \max\left\{I_Q^0 - I(x, y, z), 0.0\right\} \tag{13b}$$

To maintain the 3D LPM paradigm of only one parameter affecting dose-to-clear, the Image-In-Resist clipping intensity is defined as

$$I_Q^0 = \frac{E_0}{E} \cdot R_Q \cdot e^{-\alpha \cdot d} \tag{14}$$

where E_0 is the dose-to-clear parameter, E is the applied exposure dose, α is the resist absorbance parameter and d is the resist thickness. R_Q is the base loading parameter. It is defined as the relative amount of energy quenched at the bottom of the resist for a dose-to-clear exposure. This definition of the clipping intensity allows $0 < R_Q \leq 1$ while maintaining a constant E_0. For very thin resists the absorbance term is unity and the clipped intensity I_Q^0 is in aerial image units.

The two Image-In-Resist terms I_A and I_Q are allowed to diffuse and quench each other. The coupled set of differential Equations (15a,b) now define the CA-LPM's post exposure bake model. Following the Lammers' approach, the acid component of the Image-In-Resist is integrated through time (15c) to determine the final soluble image S at each position.

$$\frac{dI_A}{dt} = -k_Q \cdot I_A \cdot I_Q + D_A \nabla^2 I_A \tag{15a}$$

$$\frac{dI_Q}{dt} = -k_Q \cdot I_A \cdot I_Q + D_Q \nabla^2 I_Q \tag{15b}$$

$$S(\mathbf{x}) = \int I_A(\mathbf{x}, t)dt \tag{15c}$$

For the model presented here, it is assumed that $k_Q >> 1$ for instantaneous quenching. D_A and D_Q are the diffusion coefficients for the Acid and Base images respectively. The diffusion coefficients can be given as diffusion lengths to remove the PEB time variable.

$$L_A = \sqrt{2D_A t} \tag{17}$$

$$L_Q = \sqrt{2D_Q t}$$

After integrating I_A through time to obtain S, the 3D resist profile is obtained by performing a 3D develop calculation. The develop rate function is defined using the 3D-LPM contrast function and the integrated acid image.

$$\text{Develop Rate}(\mathbf{x}) = R_0 \cdot \left(\frac{E}{E_0}\right)^{\pm\gamma} \cdot S(\mathbf{x})^{\pm\gamma} + R_{min} \tag{18a}$$

The only develop parameters for the model are γ and R_{min}. R_0 is obtained by requiring the time-to-clear to equal the develop time, t_{dev} at the dose-to-clear. R_0 can then be calculated numerically using Equation 18.

$$\text{Time to Clear} = \int_0^d \frac{1.0}{R_0 \cdot \left(\frac{E}{E_0}\right)^{\gamma} \cdot \left(e^{-\alpha \cdot z} - R_Q e^{-\alpha \cdot d}\right)^{\gamma} + R_{min}} dz \tag{18b}$$

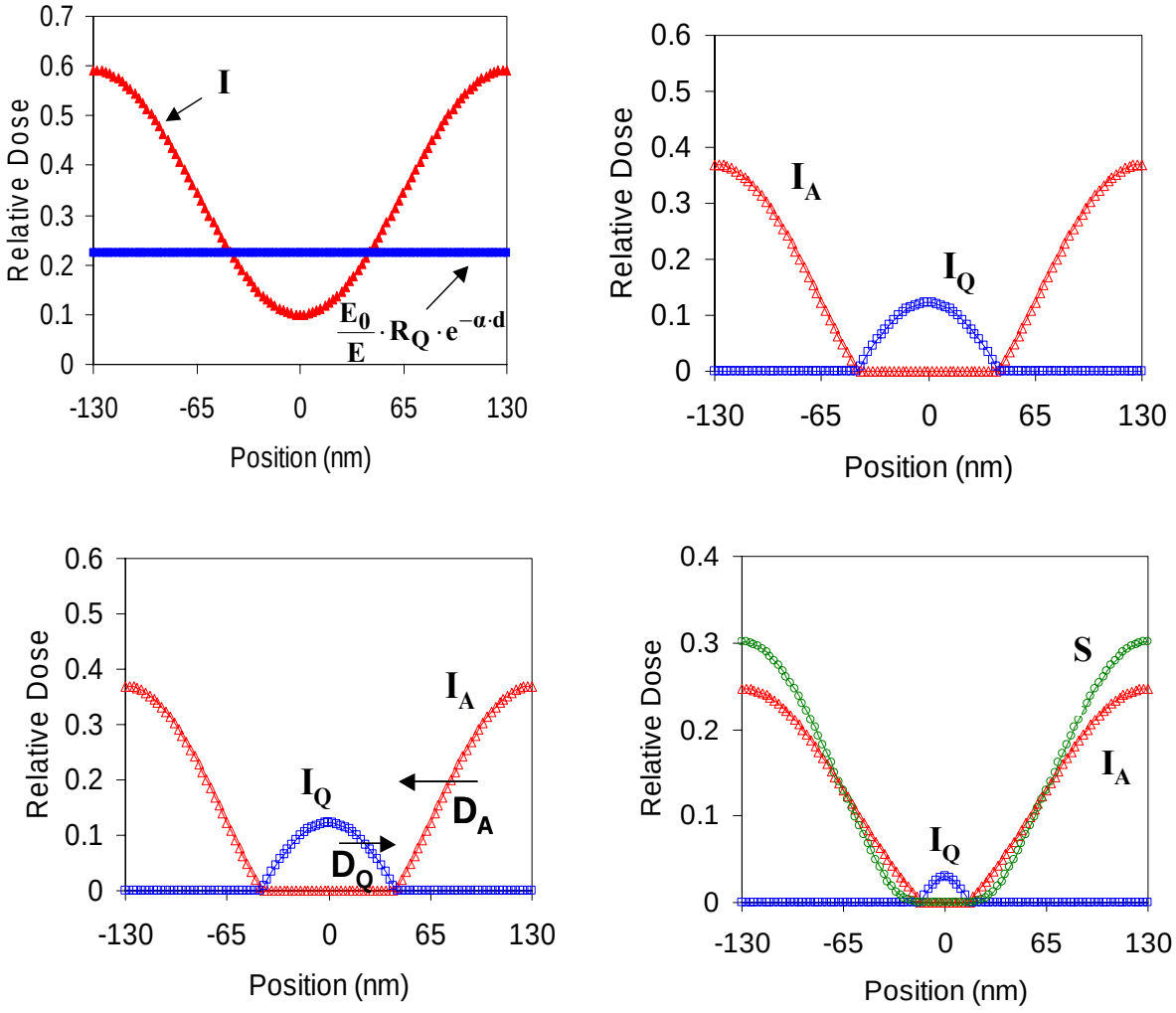

Figure 2: Representation of the PEB process for the proposed lumped parameter model for chemically amplified resists (CA-LPM). Upper Left: The initial Image-in-Resist (I) and scaled base loading . Upper Right: The clipped acid image (I_A) and base image (I_Q) before the diffusion-quenching process. Lower Left: Diffusion-Quenching Process. Lower Right: Final acid image (I_A) , base image (I_Q) , and the generated soluble image (S).

3. SOLUTION METHODOLOGY

Implementation of this model requires a fast calculation of the soluble resist fraction S(**x**) given by Equations 15a-c. Finite difference time domain (FDTD) methods are normally used to solve such nonlinear partial differential equations. Using FDTD the initial value for I_A and I_Q can be accurately marched through time. Numerical integration of $I_A(t)$ will then provide S(**x**). For this work Bode's rule for integration was used as the time integrator.

FDTD methods can generate accurate solutions but require significant computational times. Given the empirical nature of the proposed model, less accurate methods for calculating S(**x**) may be acceptable. One solution method investigated is the Operator Splitting method. Written in matrix form the couple set of Equations 15a and 15b are

$$\frac{d}{dt}\begin{bmatrix} I_A \\ I_Q \end{bmatrix} = \begin{bmatrix} D_A\nabla^2 & -k_Q I_Q \\ -k_Q I_A & D_Q\nabla^2 \end{bmatrix} \times \begin{bmatrix} I_A \\ I_Q \end{bmatrix} = \mathbf{W} \times \begin{bmatrix} I_A \\ I_Q \end{bmatrix} \tag{19}$$

where the operator **W** is nonlinear and nonsymmetrical. In the Operator Splitting method the matrix **W** is split into two separate matrices **D** and **Q.** Each matrix represents the separate diffusion and quenching operators.

$$\frac{d}{dt}\begin{bmatrix} I_A \\ I_Q \end{bmatrix} = \begin{bmatrix} D_A\nabla^2 & 0 \\ 0 & D_Q\nabla^2 \end{bmatrix} \times \begin{bmatrix} I_A \\ I_Q \end{bmatrix} + \begin{bmatrix} 0 & -k_Q I_Q \\ -k_Q I_A & 0 \end{bmatrix} \times \begin{bmatrix} I_A \\ I_Q \end{bmatrix} = \mathbf{D} \times \begin{bmatrix} I_A \\ I_Q \end{bmatrix} + \mathbf{Q} \times \begin{bmatrix} I_A \\ I_Q \end{bmatrix} \tag{20}$$

The two separate decoupled problems

$$\frac{d}{dt}\begin{bmatrix} I_A \\ I_Q \end{bmatrix} = \mathbf{D} \times \begin{bmatrix} I_A \\ I_Q \end{bmatrix} \tag{21a}$$

and

$$\frac{d}{dt}\begin{bmatrix} I_A \\ I_Q \end{bmatrix} = \mathbf{Q} \times \begin{bmatrix} I_A \\ I_Q \end{bmatrix} \tag{21b}$$

are easily solved using a Greens function for problem 21a and direct integration for problem 21b.

$$D^{-1}(\Delta t) = \begin{bmatrix} \dfrac{1}{\left(4\pi \cdot D_A \cdot \Delta t\right)^{3/2}} \iiint I_A(\mathbf{x}, t) \cdot e^{-\frac{\|\mathbf{x}-\mathbf{x}'\|^2}{4D_A \cdot \Delta t}} d\mathbf{x}' \\ \dfrac{1}{\left(4\pi \cdot D_Q \cdot \Delta t\right)^{3/2}} \iiint I_Q(\mathbf{x}, t) \cdot e^{-\frac{\|\mathbf{x}-\mathbf{x}'\|^2}{4D_Q \cdot \Delta t}} d\mathbf{x}' \end{bmatrix} \tag{22a}$$

$$Q^{-1}(\Delta t) = \begin{bmatrix} \dfrac{I_A(t) - I_Q(t)}{1 - \dfrac{I_Q}{I_A} e^{-k_Q \cdot \left(I_A(t) - I_Q(t)\right) \Delta t}} \\ \dfrac{I_Q(t) - I_A(t)}{1 - \dfrac{I_A}{I_Q} e^{-k_Q \cdot \left(I_Q(t) - I_A(t)\right) \Delta t}} \end{bmatrix} \tag{22b}$$

These solutions to the decoupled problems are exact for the any time step. The solution to the full problem 20 can be approximated by the sequential application of the two solutions 22a and 22b for iterative time steps.

$$\begin{bmatrix} I_A(t + \Delta t) \\ I_Q(t + \Delta t) \end{bmatrix} = Q^{-1}\left\{ D^{-1}\left\{ \begin{bmatrix} I_A(t) \\ I_Q(t) \end{bmatrix}, \Delta t \right\}, \Delta t \right\} \tag{23}$$

The error in this method increases with time step Δt but the solution will converge to FDTD in the limit of very small time steps. As with the FDTD method, the soluble fraction S(**x**) can be obtained using the appropriate time integrator on the resulting $I_A(t)$. For this work we investigated using 1, 4, and 16 time steps. The resulting algorithms are labeled OS-1, OS-4, and OS-16 respectively. Additionally, the algorithm OS-0 is also used for comparison. In this algorithm the soluble image is obtained without time integration. Instead the final acid image after diffusion and quenching with a single time step is used.

An alternate solution method for obtaining S(**x**) arises when one considers the case with zero quencher.

$$\frac{dI_A}{dt} = D_A \nabla^2 I_A \tag{24a}$$

$$S(\mathbf{x}) = \int I_A(\mathbf{x}, t)dt \tag{24b}$$

The soluble image S(**x**) can then be written as a direct convolution of a Green's function $K_A(t)$ with the initial Acid Image $I_A(t=0)$.

$$S(\mathbf{x}) = \iiint I_A(\mathbf{x}, t=0) K_A(\mathbf{x}-\mathbf{x}')d\mathbf{x}' \tag{25a}$$

where in three dimensions

$$K_A(x-x', t) = \frac{1}{(2\pi)^{3/2}} \int_0^t \frac{e^{\frac{-\|x-x'\|^2}{4D_A t}}}{(2 \cdot D_A \cdot t)^{3/2}} dt \tag{25b}$$

The resulting S(**x**) is exact for the zero quencher case. Researchers at IBM [16] determined this impulse response for chemically amplification using Monte-Carlo simulations. The IBM group suggested a Lorentzian functional form for this impulse response. As shown in Figure 3 the Green's function given by Equation 25b is close to a Lorentzian however that approximation is not exact. Although this expression will yield exact results for the zero quencher case the results do not work when base is present. However it is possible to formulate an approximate solution, $\tilde{S}(\mathbf{x})$, to the problem that includes the solution given by Equation 25 and a single correction factor. The correction factor is written as a convolution with the initial base image.

$$\tilde{S}(\mathbf{x}) = \int I_A(\mathbf{x}, t)dt = \iiint I_A(\mathbf{x}, t=0) K_A(\mathbf{x}-\mathbf{x}')d\mathbf{x}' - \iiint I_Q(\mathbf{x}, t=0) K_Q(\mathbf{x}-\mathbf{x}')d\mathbf{x}' \tag{26}$$

The trick of course is to determine the best kernal functions K_A and K_Q that minimize the deviations between $\tilde{S}(\mathbf{x})$ and the true S(**x**). For this work we took the easy way out and arbitrarily used the form given by Equation 25b for both K_A and K_Q. The resulting solution method is termed the Modified Kernal Approximation (MKA). The time integration to achieve the soluble image $\tilde{S}(\mathbf{x})$ is implicit and only one time step is required.

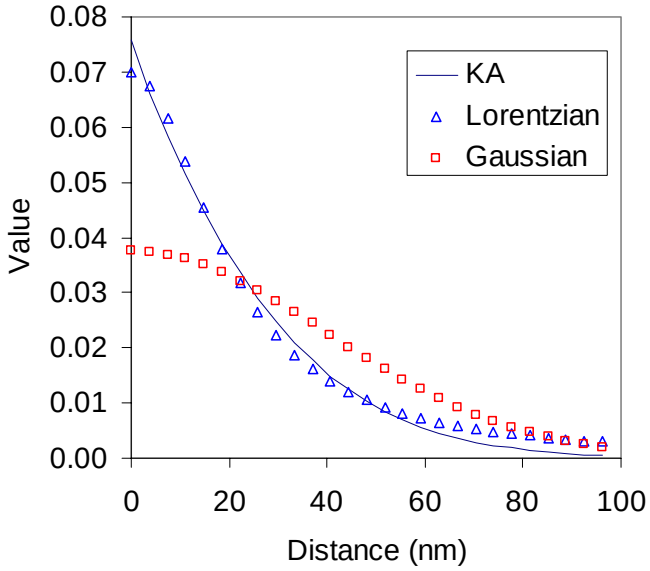

Figure 3: Comparison of 3D impulse response function for diffusion-amplification process, K_A from Equation 25b, with the best fit Lorenztian function. $D_A = 13nm^2/s$ and PEB time 60s . Also shown is the 3D Gaussian function for the same conditions.

4. RESULTS AND DISCUSSION

The goal of the new CA-LPM model is to yield the best agreement to a full physical resist model. To this end a standard 193nm chemically amplified resist model was used. The model resist was selected because the base diffusion parameter was large enough to affect the isofocal position for the dense images. This is the type of resist for which the standard 3DLPM model generates poor results. The model parameters for the full physical model are given in Table 1. The imaging condition was 130nm equal lines and spaces with binary mask, 193nm exposure with 0.68 NA and 0.7 sigma partial coherence. All simulations were all performed using PROLITHv8.03. All parameters not shown in Table 1 but included in the full PROLITH model were turned off in the simulation. The parameters used for the CA-LPM model are also shown in Table 1. The CA-LPM parameters were derived analytically from the full CA resist parameters and process conditions.

Table 1: Modeling parameters used for comparison of CA-LPM with full physical Chemically amplified resist model in PROLITH v8.03. Left: Full Physical PROLITH model for Chemically amplified resists. Right: CA-LPM model

Parameter	Value
n	1.699
A (um^{-1})	0
B (um^{-1})	1
C (cm^2/mJ)	0.05
k_a	0.3
D_A (nm^2/s)	10
[Q]	0.125
D_Q (nm^2/s)	40
R_{max} (nm/s)	500
R_{min} (nm/s)	0.05
R_n	12

Parameter	Value
n	1.699
α (um^{-1})	1
E_0 (mJ/cm^2)	4.15
L_A (nm)	35
R_Q	0.75
L_Q (nm)	69
γ	12
R_{min} (nm/s)	0.05

Using the model described above, the accuracy of the different solution methods was tested. First, the soluble image, S(**x**), near the mask edge was compared. The results for all solution methods are shown in Figure 4. The results are for the bottom of the resist at the dose to size condition. Also in Figure 4 the deviations from the FDTD result for the different approximate solution methods are shown. Positive error values occur when the approximate solution method over-estimates the soluble image and negative errors occur when the soluble image is under-estimated. Exact match across the entire image is desired but accuracy near the mask edge is the most critical region. As demonstrated, both the OS-16 and the OS-4 have reasonable accuracy near the mask edge. The MKA model achieves better results than the OS-1 model for the same computational effort but both are less accurate than the higher order OS-n methods. The poor results for the OS-0 model reiterates the necessity to integrate the acid image to achieve acceptable results.

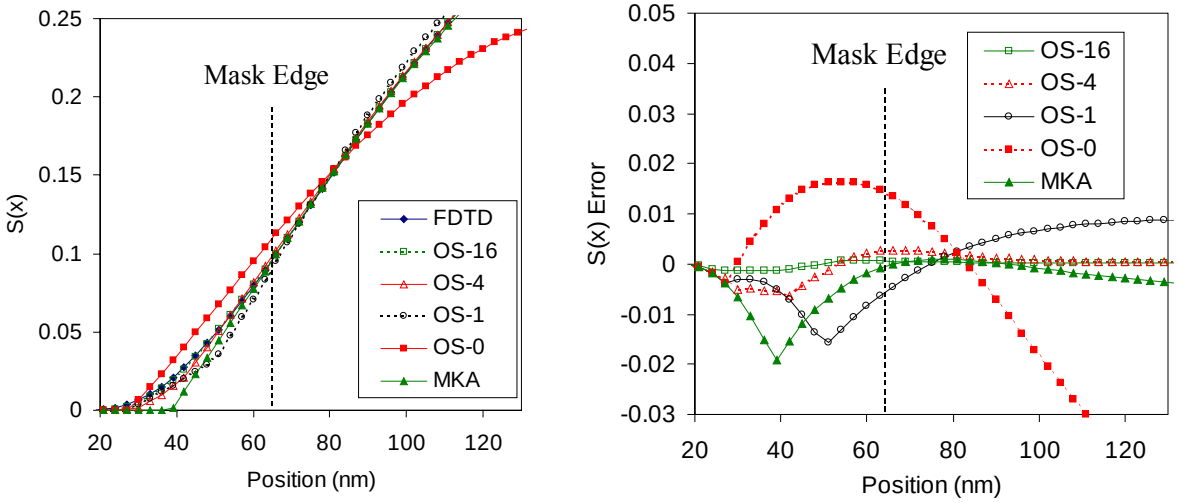

Figure 4: Comparison of generated soluble image near mask edge for 1D problem using various solution methods. Left: Soluble image as a function of position. Right: Deviation from FDTD method for approximate methods.

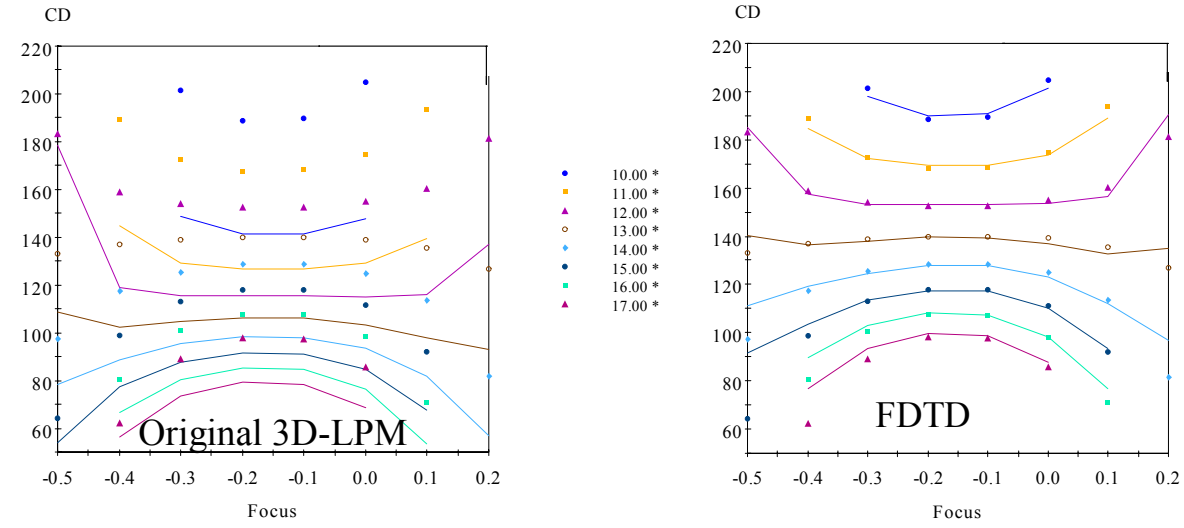

Figure 5: Comparison of simulated focus exposure data generated using the full chemically amplified resist model (symbols) with the LPM model (lines). Left: Standard 3D-LPM results. Right CA-LPM model results using the FDTD solution method.

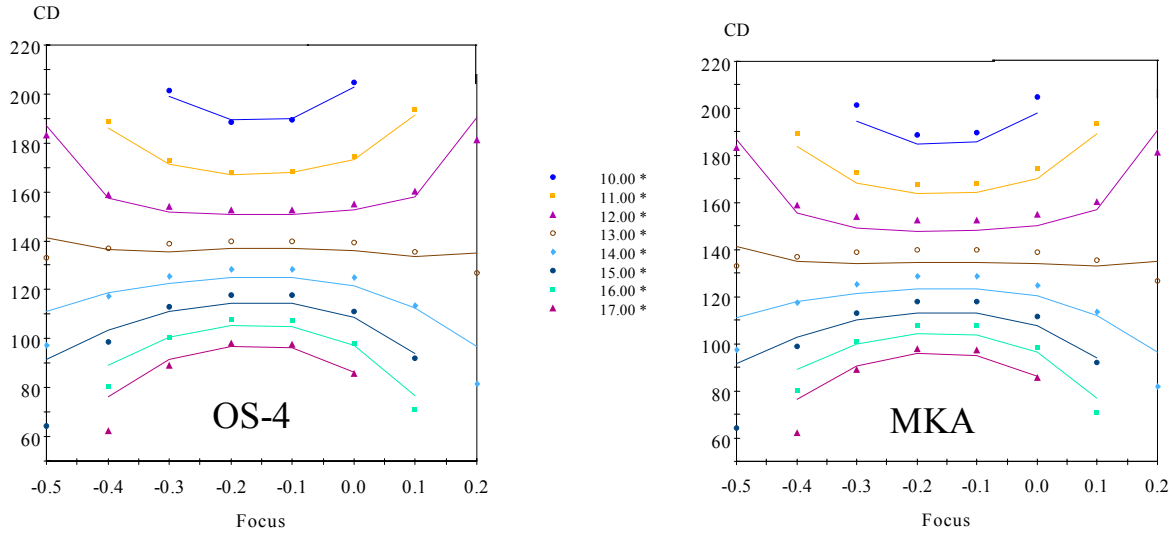

Figure 6: Comparison of various approximate solution methods for the CA-LPM model with the original chemically amplified resist focus exposure results. Left: OS-4 Right MKA

Figures 5 and 6 compare various approximate solution methods for the CA-LPM model with the original chemically amplified resist focus-exposure results. Obviously, the original LPM, with no base quenching, does much worse than the three CA-LPM models shown.

5. CONCLUSION

In this paper the Lumped Parameter Model was extended to explicitly include chemically amplified resist effects. The new model, CA-LPM, includes base clipping of the Image-in-Resist into separate acid and base images. The acid and base images simultaneously diffuse and quench each other. The final develop rate within the resist is a function of the average acid image during this diffusion-quenching process. The standard LPM two term develop rate function was used to capture develop contrast. The final model should have better matching to chemically amplified resists than the previous 3D-LPM model.

Various solution methods for the diffusion-quenching process were investigated. It was found that the proper solution of the diffusion-quenching equations are required to achieve good results. Both the multiple step Operator Splitting method and the FDTD method yielded comparable results. The single time step methods with a Gaussian diffusion kernal yielded poor results. The single step Modified Kernal Approximation method, as proposed in this paper, yielded better results but this method's performance for all imaging conditions was not tested.

REFERENCES

1. M.D. Smith, J.D. Byers, C.A. Mack, A *Comparison Between the Process Windows Calculated with Full and Simplified Resist Models*, Optical Microlithography XV, Proc SPIE vol 4691, (2003) pp 1199-1210.
2. N. Cobb, A. Zakhor, M. Reihani, F. Jahansooz, V. Raghavan, Optical Microlithography X, Proc. SPIE vol 5040, (2003) pp 458-468.
3. Y. Granik, N. Cobb, T. Do, *New Process Models for OPC at sub-90nm Nodes*, Optical Microlithography XVI , Proc. SPIE vol 3051, (2003) pp 1166-1175.
4. C. Ahn, H. Kim, K. Baik, *A Novel Approximate Model for Resist Processes*, Optical Microlithography XI , Proc. SPIE vol 3334, (2003) pp 752-763.
5. D. Fuard, P. Schiavone, *Assessment of Different Simplified Resist Models*, Optical Microlithography XV, Proc SPIE 4691, (2003), pp1266-1277.

6. H. Fukuda, K. Hattori, T. Hagiwara, *Impact of Acid/Quencher Behavior on Lithography Performance,* Optical Microlithography XIV vol 4346, (2001) pp 319-330.
7. D. Van Steenwinckel. , J. H. Lammers, *Enhanced Processing: sub-50nm Features with 0.8 micron DOF Using a Binary Reticle,* Advances In Resist Technology and Processing XX , Proc. SPIE vol 5039, (2003) pp 225-239.
8. B. TollKuhn, D. Matiut, *Resist Models and Calibration, What Leads to Predictive Results*, 1th IISB Lithography Simulation Workshop, Hersbruck, 2003.
9. J.H. Lammers, *Acid Quencher Reaction Diffusion during the Post Exposure Bake of Chemically Amplified Resists*, Phillips Research Report, PRLe UR 2001/817 (2001).
10. C.A. Mack, A. Stephanakis, R. Hershel, Kodak Microelectronics Seminar, Proc. (1986) pp 228-238.
11. C.A. Mack, Optical Microlithography VII, Proc SPIE vol 21976, (1994) pp 501-510.
12. T.A. Brunner, R.A. Ferguson, Optical Microlithography IX, Proc SPIE vol 2726, (1996) pp 198-207.
13. J. Byers, M. Smith, C.A. Mack, *3D Lumped Parameter Model for Lithographic Simulations,* Optical Microlithography XV, Proc. SPIE vol 4691, (2002) pp 125-137.
14. J. Malov, C. Kalus, T. Schmoller, R. Wildfeuer, *Accuracy of New Analytical Models for Resist Formation Lithography*, Optical Microlithography XV, Proc. SPIE vol 4691, (2002) pp 1254-1266.
15. M.D. Smith, J.D. Byers, C.A. Mack, Advances In Resist Technology XXII, Proc SPIE vol 4691, (2004).
16. F.H. Dill, W.P. Hornberger, P.S. Hauge, J.M. Shaw, IEEE Trans. Electron Devices , **ED22**, 445 (1975).
17. W. Hinsberg, F. Houle, M. Sanchez,. J. Hoffnagle, G. Wallraff, D. Medeiros, G. Gallatin, J. Cobb, *Extendibility of Chemically Amplified Resists: Another Brick Wall?*, Advances In Resist Technology and Processing XX, Proc. SPIE vol 5039, (2003) pp 1-14.